PHOTONICS Research

Electrically active and thermally passive liquid-crystal device toward smart glass

Guan-Fu Sung,[1] Po-Chang Wu,[2] Victor Ya. Zyryanov,[3] and Wei Lee[2,*]

[1]College of Photonics, National Yang Ming Chiao Tung University, Tainan 711010, Taiwan
[2]Institute of Imaging and Biomedical Photonics, National Yang Ming Chiao Tung University, Tainan 711010, Taiwan
[3]Kirensky Institute of Physics, Federal Research Center "Krasnoyarsk Scientific Center," Siberian Branch of the Russian Academy of Sciences, Krasnoyarsk 660036, Russia
*Corresponding author: wei.lee@nycu.edu.tw

Received 14 July 2021; revised 30 August 2021; accepted 7 September 2021; posted 9 September 2021 (Doc. ID 437654); published 28 October 2021

Cholesteric liquid crystals (CLCs) are an important soft material for display and sensing technologies due to their unique optical and thermal properties, which are susceptible to external perturbations such as the electric field and temperature variation. The typically periodic structure of a CLC with a twist between molecular layers permits its chiral photonic crystallinity and the resulting selective reflection of a bandwidth in the otherwise generally high transmission spectrum of incident light. Here we report on a novel dual-mode CLC device as smart glass that enables the transparency to be self-adaptive to temperature and is simultaneously characterized by a fully on-demand, electrically controlled function, allowing users to regulate the suitable or desired extent of transparency in accordance with their living climate zones or personal needs. The working principle is based on the controllable strength of voltage-induced electrohydrodynamic flow, generating temperature-dependent dynamic scattering for passive control. Moreover, the transmission can be reversibly modulated and switched by applied AC voltage for active control between the transparent and opaque states. As a proof of concept, the characteristic Bragg reflection can be designed to sit in the near-infrared region to partially block unwanted thermal radiation in the optically transparent state.

https://doi.org/10.1364/PRJ.437654

1. INTRODUCTION

It has been known since the 1970s that the orientation pattern of nematic liquid crystal (LC) possessing negative dielectric anisotropy ($\varepsilon_{\parallel} < \varepsilon_{\perp}$) and positive anisotropy in conductivity ($\sigma_{\parallel} > \sigma_{\perp}$) can be readily generated and manipulated by the magnetic or electric field [1]. Often observed under a polarizing optical microscope (POM), distinct domain structures or distorted patterns of the LC director, viz., the local average molecular axis, originate from circular or turbulent motions of the impregnated free space charges or ions in response to an applied AC electric field at extensive voltages ranging from a few volts to a hundred volts and frequencies spanning between ~1 Hz and several kilohertz, thereby leading to electrohydrodynamic (EHD) flow [2]. Steady textural patterns named Williams domains presenting orientationally periodic distribution of nematic alignment have been well documented in the condition of a narrow range of low voltages beyond a threshold [3,4]. At higher AC voltages, however, the EHD flow becomes intense, creating a complex, fluctuating director configuration to incur dynamic scattering (DS). With regard to the related condition between applied voltage V and applied frequency f, an f–V critical boundary granting the initially unperturbed transparent state to transform can be designated in both conduction and dielectric regimes [5,6]. Moreover, transparency tunability can be realized by means of the modulated voltage-dependent DS strength, until a saturated opaque state is reached at a high voltage in a favorably low-frequency range where the transmission virtually vanishes. Our previous study on identification of the optimal frequency range for the EHD induction of the cholesteric uniform lying helix structure connotes that the ion density, in addition to the amplitude and frequency of the operating voltage, plays an important role in controlling the transmitted radiance of scattered light [7].

Several optical textures resulting from the EHD effect have been employed to regulate split laser beams by constructing tunable diffraction gratings and maneuvering different control parameters such as the driving frequency, voltage, and cell gap [8]. Based on the EHD effect, the switching of the LC optical state to the DS state has been suggested for the use of smart windows as a potential application of electro-optical responses [9–13] owing to many advantages such as fast response, high contrast ratio, low applied electric field intensity (for achiral nematic LC), and wide viewing angle with effective switching

for thousands of times [9]. A rapid switching in the sub-second scale is achievable by directly increasing the applied field to avoid the delay time [11]. Compared with dielectrically positive LC (which exhibits positive dielectric anisotropy), negative LC yields stronger light scattering at voltages exceeding the threshold voltage V_{th}, permitting two distinctive, reversibly switchable transmission states—transparent and opaque—with a higher contrast ratio [14]. In a study of dichroic dye-doped LC systems including a cholesteric LC (CLC) and a nematic LC dispersed with tetrabutylammonium bromide (TBAB), it was found that the added ions (i.e., TBAB) promoted the contrast for LC window devices based on the EHD mechanism [15]. A dual-frequency (DF) switching smart window manifested with a DF-CLC containing ionic liquid was investigated under the application of electric signal at 20 Hz–10 kHz to control the EHD magnitude [10].

Automatic devices capable of sensing and responding to environmental conditions are considered as an application of intelligent technique. A self-shading approach of a smart window as a light shutter was proposed on the basis of a dichroic dye-doped LC whose light scattering state (with specular transmittance T_s% of ~20%) in the CLC phase can be thermally and optically induced from the transparent state (with T_s% of ~65%) in the SmA* phase through phase transition and ultraviolet (UV) exposure of azobenzene molecules in dye-doped CLC, respectively [16]. Similarly, under a remote stimulation by UV radiation to drive EHD instabilities, a photochromic dye was utilized in a complex LC material system to render photoinduced charge carriers, fashioning reversable, double optical states including the green light-commanded state as the counterpart (i.e., transparent) one [17]. Clearly, employing azobenzene or photochromic dye in self-switching LC smart windows empowers sensing UV radiation and the subsequent suppression of optical transmission. Although the absorption of incident light by dichroic dyes in LC has been dealt with in many applications, the maximal transmittance (T%) in the transparent state is intrinsically low [16]. Also, azobenzene smart windows once switching to the "opaque" state in response to the UV component of terrestrial radiation can hardly reverse back to the transparent state until the UV radiation diminishes (e.g., at sunset). On the other hand, the practical use of a smart window containing photochromic dye to ensure reversible switching operations [17] would rely on solar green and UV light. It would become uncontrollable in that the solar spectrum is constituted by green light along with UV radiation.

Electrical control with a deterministic threshold electric field to prompt the onset of LC convective instability helps one grasp the transmission behaviors in various f–V operating regions. In general, the transparent and DS regimes can be set apart with a threshold boundary. Variable DS strengths giving rise to different degrees of T% and, in turn, distinct levels of opacity including a tunable translucent state and an opaque state with minimally saturated T% can be sought by a thorough analysis of three f–V zones for the transparent, graded translucent, and opaque states to result. This study introduces a dual-mode, passive and active, smart glass based on the EHD effect stemming from the mass flow of negative CLC molecules caused by ion motion responsive to low-frequency (<1 kHz) voltage. The strong dependence of transmission on temperature T and applied AC field underlies the working principle for the reported smart glass. Without any UV treatment process or the need to incorporate extra nonmesogenic substances, thermally passive or adaptive switching is clarified between the transparent and opaque states, and more options are fulfilled for graded transmission in the translucent state. We also examined the electrically active control as well as the consequent transmission characteristics in the three states and identified the f–V boundaries of V_{DS} that divided the EHD realm into opaque and translucent zones and of V_{th} that separates translucent and transparent zones. To demonstrate a conceptually value-added implement for energy conservation, the pitch length for the electrically unperturbed CLC was designed to allow Bragg reflection to fall in the near-infrared (NIR) region so that the window can substantially reflect solar thermal radiation while it is transparent in the visible spectrum. We report in this work what is, to the best of our knowledge, the first manifestation of a CLC smart window featuring reversible, electrical tuning of a T-dependent opaque state without having to change the material composition or attach additional components [18,19]. By setting the V and f values for a desired temperature T_{DS} at which riotous DS takes place, this temperature adaptation avails a smart window suitable vastly in various climate zones.

2. EXPERIMENT

In this study the host nematic LC DV-10001 (Daily Polymer, Taiwan) used possesses birefringence of 0.200, dielectric anisotropy of −5.4, resistivity of $3.0 \times 10^{11}\ \Omega \cdot \mathrm{cm}$ at room temperature, and clearing point of 109.0°C ± 0.5°C. The negative nematic host is a eutectic mixture consisting of plural neutral and polar single compounds. Adding with the left-handed dopant S-811 (Yung Zip Chemical, Taiwan) by the component ratio of DV-10001 : S-811 = 86.21% : 13.79% (ratio of mass fractions) turned the nematic LC chiral, resulting in a left-handed CLC exhibiting the Bragg reflection centered at the wavelength λ_c of c.a. 1050 nm. The doped mixture was vigorously stirred at 120°C in isotropic phase for 2 h to make a homogeneous blend and then filled into empty cells by capillary action. Each cell comprises a pair of indium–tin-oxide glass substrates whose inner surfaces were coated with polyimide (SE-2170, Nissan Chemical, Japan) treated in an antiparallel rubbing process to promote a strong planar alignment with a small tilt (~2°) for the CLC in the initial Grandjean planar (GP) configuration. The cell gap is 15.0 ± 0.5 μm, and the overlapped electrode area is 0.25 cm^2. Various optical textures of a sealed CLC cell produced by the EHD effect at various agitating voltages were monitored with a POM (Olympus BX51) in the crossed-polarizer transmission mode. Under precision temperature control (Linkam T95-PE) in thermal equilibrium, optical transmission spectra were acquired with a fiber-optic spectrometer (Ocean Optics HR2000-Plus) together with a tungsten halogen light source (Ocean Optics HL-2000). To extend the measurement to longer wavelengths (900–1600 nm), another fiber-optic spectrometric system, composed of an AvaSpec-NIR256-1.7-EVO spectrometer and an AvaLight-HAL-S-Mini tungsten halogen light source, was also

employed. The CLC cell was connected to a function generator (Tektronix AFG-3022B) in conjunction with a power amplifier (TREK Model 603). Voltage- and temperature-dependent transmission was examined by placing the sample on a temperature controller (TEC Controller CDS15008RRA) and between a He–Ne laser source (operating at wavelength λ of 632.8 nm) and a photodetector without polarizers. Here, the probe light, LC cell, and detector were set in the same axis. The light intensity directly received by the detector without a cell inserted in the optical path was normalized to 100%. The cell and the detector were separated by a sufficient distance such as 10 cm in the spectral measurement and 50 cm in the voltage- and temperature-dependent transmission measurement. Accordingly, transmittance (T%) discussed in this study can be identically regarded as specular transmission unless explicitly specified. To test the thermal tuning in practice and record the thermal image in a real-time observation, an IR camera (FLIR ThermaCam E4) was exploited.

3. RESULTS AND DISCUSSION

The sandwiched CLC samples were fabricated in the GP texture as the initial and stable state. The self-assembled helical structure allowed a small rotational offset of the anisotropic unit from its neighboring layers to yield the Bragg reflection whose central wavelength, when observed along the helical axis, can be described by

$$\lambda_c = p \cdot n_{\text{avg}}, \tag{1}$$

where the pitch length p is the distance along the helix over which a full (or 2π) rotation is completed, and n_{avg} denotes the average refractive index of the cholesteric phase. The transparent GP state was first verified without external voltage. To illustrate the mechanisms for the said dual-active control mode (by both V and f) and passive control mode (by T due to exposure to solar thermal heating), Fig. 1 shows a self-explanatory schematic for the operation. With a voltage control by increasing 100-Hz V from 0 to $30V_{\text{rms}}$ at a fixed temperature ($T = 30$°C), the induced EHD effect can drive the optical state away from its naturally stable GP state. Furthermore, for frequency control, increasing f from 100 to 300 Hz at the applied voltage of $30V_{\text{rms}}$ reverts the optical state from the hazy to transparent state [Fig. 1(a)]. On the instance of passive control as shown in Fig. 1(b), elevated T from 20°C to 30°C or higher at a fixed applied voltage ($V = 30V_{\text{rms}}$ and $f = 100$ Hz) can also arouse EHD flow, leading to the transformation from the transparent to translucent or opaque state.

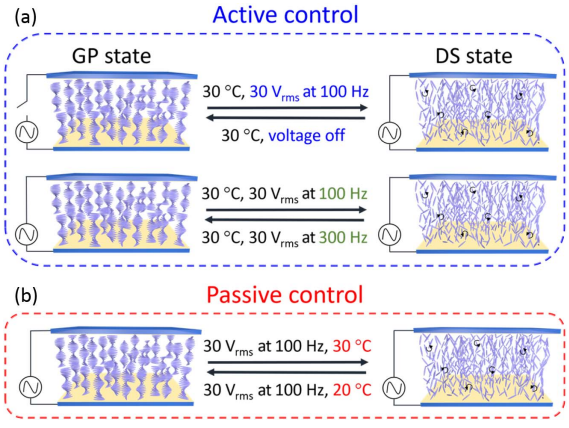

Fig. 1. (a) Active control by switching on/off a voltage or by altering the frequency of the AC voltage. (b) Passive control enabled by the temperature change at a fixed voltage.

Figure 2 delineates the architecture and working mechanism of the proposed thermo-responsive CLC window for adaptive smart switching. When the local temperature is comfortable or incident solar radiation is mild, the CLC glass remains transparent for incident visible light, whereas the reflecting part of solar thermal radiation is at null voltage. As a matter of fact, this function is preserved regardless of the weather condition as long as the voltage is turned off [see Fig. 2(a)]. To assess the feasibility, we built an extreme condition where the sunlight after passing the CLC cell and an empty cell with the same effective area of 1.8 cm^2 was imposed on a black Bristol cardboard. After 210 min (11:00–14:30) of sunlight exposure on a sunny day, our pretests confirmed that the temperature in the position behind the IR-reflective CLC cell in the GP state was 40.8°C, which was ~5°C lower than that (at 45.6°C) at an adjacent position behind the empty cell. The idea of applying the GP state of the proposed CLC smart glass with an IR-reflection optical feature for lowering indoor temperature is alternatively supported by some previous works that suggest various approaches toward promoting energy saving efficacy in buildings by electrically tunable broadband IR reflection through polymer stabilization [20,21] or by hyper-IR reflection with a bilayer configuration [22]. In contrast, Fig. 2(b) shows how the CLC smart window works on a hot sunny day with severe solar irradiance or when the temperature is uncomfortably high. Solar heating induces the EHD effect after the CLC under the application of external AC voltage absorbs enough thermal radiation to elicit the DS state, thereby obstructing the sunlight

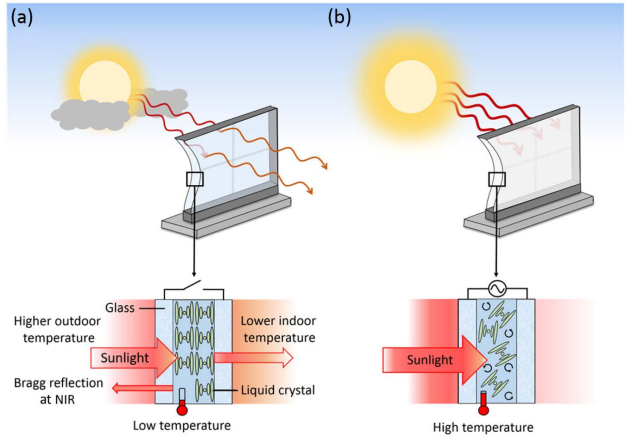

Fig. 2. Schematic explication of the CLC cell as a smart window. (a) At a moderate temperature, the electrically unperturbed CLC exhibits the GP configuration, giving the transparency in the visible while partially reflecting the incident NIR radiation via Bragg reflection. (b) At a high surrounding temperature outdoors, solar heating from terrestrial radiation causes EHD flow in the CLC under the application of AC voltage. The CLC molecules in an unstable or irregular arrangement to procure the DS or opaque state will strongly scatter the incident sunlight.

(in the visible and NIR spectrum) to penetrate into the room. Aside from the tunable and switchable shading, the function of personal privacy protection can be achieved as the smart glass operates in the DS state. As such, this study is aimed to experimentally illustrate and theoretically explain the detailed properties of the smart window in the following text.

Figure 3(a) displays the measured optical spectra of a CLC cell in the range of $\lambda = 400$–1600 nm at 30°C at various voltages. Here, the transmission spectrum of a piece of ITO glass showing ~89% transmittance on average in the visible regime is exhibited as a reference. Note that the maximal transmittance of light as measured in this study is ~80% after passing through a CLC cell comprising a pair of ITO-coated glass substrates. The inherent Bragg reflection in the unperturbed GP state lies within the NIR region, signifying the capable rejection of and hence reduction in transmitted thermal radiation despite the high transparency in the visible. By electrically active control to decrease f from 800 to 100 Hz at a given voltage (fixed at $V = 100V_{\text{rms}}$ in this case), the transmission in the overall visible-to-NIR spectrum dropped significantly, suggesting distorted chiral ordering or damaged or fragmented periodicity of the pitch at 800 Hz and fully disrupted CLC ordering at 100 Hz. The DS phenomena caused by the applied electric field and the resulting CLC instabilities can be observed by POM images as depicted in Fig. 3(b).

The optical transmission properties subjected to electrically active operation can be understood by analysis of the relation between $T\%$, at a representative λ in the visible range, and V as a variable. For $T\%$ being unity as a reference without a sample in the optical path, Fig. 4(a) shows $T\%$ of the CLC cell varying with V at several f values (70, 300, 500, and 600 Hz) when $T = 30$°C, revealing $T\%$ ~80% prior to EHD induction. Such a typical V – $T\%$ curve is characterized by two noticeable voltages by which the effective voltage range of the electro-optical switch can be specified. Here the threshold voltage V_{th} and the severe DS voltage V_{DS} are defined at $T\% = 79\%$ and <1%, respectively, and three transmission regions can be thus obtained: transparent (where $T\% > 79\%$), translucent ($79\% \geq T\% \geq 1\%$), and opaque ($T\% < 1\%$). For example, $V_{\text{th}} = 16V_{\text{rms}}$ and $V_{\text{DS}} = 20V_{\text{rms}}$ were determined at an operating frequency of 70 Hz. Note that each data point in a V – $T\%$ plot, collected from a transmitted He–Ne laser beam at $\lambda = 632.8$ nm, was attained after an elapsed time of 5 s to ensure the steady state throughout the cell. Furthermore, we measured transmission spectra in the wavelength range of 400–800 nm of the CLC cell driven by voltages at $f = 70$ Hz in a designated voltage range in attempt to ascertain that determining a set of V_{th} and V_{DS} at a fixed frequency by transmission at a single wavelength is appropriate or nonspecific. As shown in Fig. 4(b), the optical profiles of transmission spectra in the transparent GP state at $V < V_{\text{th}} = 16V_{\text{rms}}$ at 70 Hz and opaque DS state at $V > V_{\text{DS}} = 20V_{\text{rms}}$ at 70 Hz were nearly invariant. In contrast, a slight wavelength dependency of transmission was obtained in the spectra within the voltage range of $V_{\text{th}} < V < V_{\text{DS}}$, presumably due to the similar wavelength-dependent optical profile in the transmission spectrum of an ITO-glass substrate [Fig. 3(a)] or the formation of small domains with sizes comparable to visible wavelengths that dominated the wavelength-dependent light intensity by Rayleigh scattering. These results indicate that measuring the V – $T\%$ curves at different wavelengths could lead to moderately distinct voltage-dependent transmission properties of the cell in voltage-sustained translucent DS states, but it would not affect determining the values of V_{th} and V_{DS}, as the voltage-induced transmission change points, corresponding to the transparent-GP–translucent-DS and

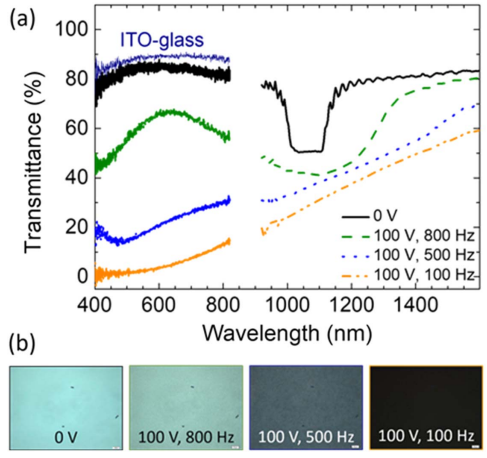

Fig. 3. (a) Transmission spectra of a single piece of ITO-glass substrate and the CLC cell at zero voltage and driven by $100V_{\text{rms}}$ at three different frequencies ($T = 30$°C) and (b) corresponding textural micrographs of the CLC sample obtained with crossed polarizers in various AC voltage conditions (scale bar: 50 μm).

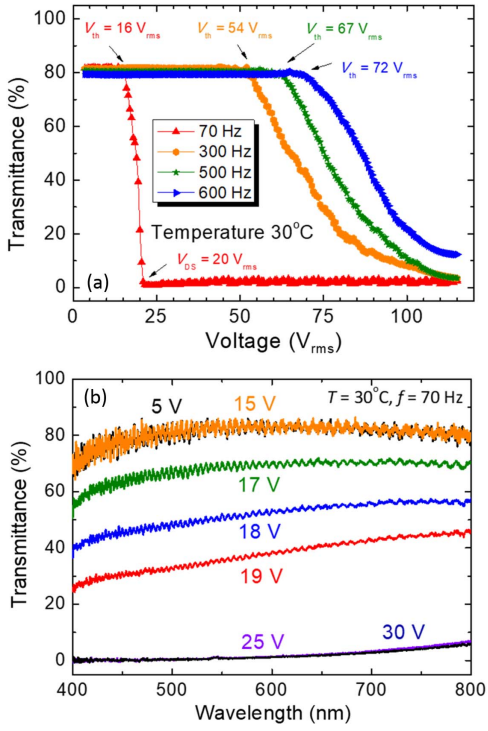

Fig. 4. (a) Voltage-dependent transmission curves (without polarizers) of the CLC cell under EHD induction at various applied frequencies. $\lambda = 632.8$ nm. (b) Transmission spectra of the CLC cell driven by various voltages at a fixed frequency of 70 Hz. The controlled ambient temperature $T = 30$°C.

translucent-DS–opaque-DS state transitions, were nearly invariant.

Figure 5 was constructed to illustrate the three transmission zones established for the designed smart window. They are the transparent GP (represented by the sapphire blue area), translucent DS (pistachio green area), and opaque DS (ocean blue area) regions, depending simultaneously on the applied voltage and frequency. These zones were categorized according to the extent of transparency or light scattering, and two DS zones can be separated in correspondence with the tunable and saturated scattering states, resulting in translucent and opaque appearances, respectively. It is noted that, by increasing V, the f-dependent translucent range becomes wider, providing more gray-level choices in transmission by tuning f. Figure 5 also indicates that a lower f favors the induction of EHD flow for DS to occur, and the higher the driving frequency, the higher the two characteristic voltages V_{th} and V_{DS} ($>V_{\mathrm{th}}$). To retain the GP transparent state under V, a maximal V and a minimal f set the limits for the driving voltage's amplitude and frequency. A theoretical treatise describing f dependence of V_{th} [23] can be adopted for comparison, which shows good agreement of our experimental data with the theoretical significance. The corresponding threshold voltage V_{th} at an excitation frequency f (as indicated by the yellow boundary line in Fig. 5) in the conduction regime is calculated by [24]

$$V_{\mathrm{th}}^2 = V_H^2\left[1 + (\zeta^2 - 1)\left(\frac{f}{f_c}\right)^2\right] \Big/ \left[1 - \left(\frac{f}{f_c}\right)^2\right], \tag{2}$$

where V_H is DC Helfrich voltage, and the unitless Helfrich parameter ζ^2 is related to the material characteristics, defined by

$$\zeta^2 = \left(1 - \frac{\varepsilon_{\parallel}}{\varepsilon_{\parallel} - \varepsilon_{\perp}} \cdot \frac{1}{1 + \eta_0/\gamma_1}\right) \cdot \left(1 - \frac{\varepsilon_{\parallel} \cdot \sigma_{\perp}}{\varepsilon_{\perp} \cdot \sigma_{\parallel}}\right), \tag{3}$$

where γ_1 represents the twist viscosity, and $\sigma_{\parallel}$ and $\sigma_{\perp}$ are the orthogonal components of conductivity. The cutoff frequency f_c appearing in Eq. (2) is expressed by

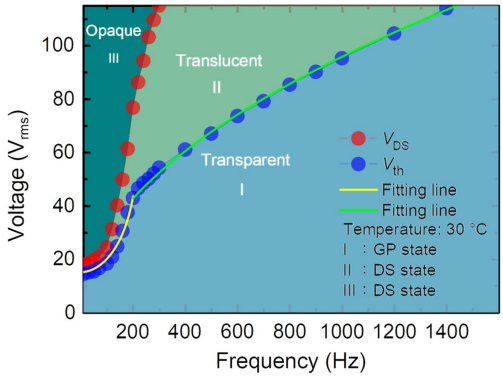

Fig. 5. Voltage and frequency dependence of three optical transmission states—transparent (or GP), translucent (or tunable DS), and opaque (namely, highly DS) regimes—distinguished by three colored areas. The two colorful curves, yellow and green, are fitted to the experimental V_{th} data represented by the blue filled circles, indicating the conducting and dielectric dominions governed by the frequency effect. The cutoff frequency f_c described in Eq. (4) determines the upper terminal of the yellow curve, and the value is approximately 200 Hz for the 30°C temperature condition.

$$f_c = \frac{1}{2\pi\tau}\sqrt{\zeta^2 - 1}, \tag{4}$$

where τ is the dielectric relaxation time, defined by

$$\tau = \frac{1}{4\pi} \cdot \frac{\varepsilon_{\parallel}}{\sigma_{\parallel}}. \tag{5}$$

η_0 in Eq. (3) can be described as

$$\eta_0 = \frac{\eta_1 + \eta_2 - \gamma_1}{2}, \tag{6}$$

where η_1 and η_2 are the Miesowicz viscosity coefficients. For the dielectric regime above the critical frequency f_c, the corresponding threshold electric field E_{th} varies with f in the following form [25,26]:

$$E_{\mathrm{th}} = \frac{2}{\zeta}\sqrt{\frac{2\pi f}{\Lambda}}, \tag{7}$$

where Λ has the reciprocal dimension of viscosity. Equation (7) indicates that E_{th} is proportional to the square root of f (that is, $E_{\mathrm{th}}^2 \propto f$) based on a parabolic law, giving the green boundary curve in Fig. 5. Accordingly, by virtue of the frequency-dependent V_{th} and V_{DS}, the proposed dual-active control scheme can be implemented, and voltage conditions suggested in Fig. 1(a) are valid for electrical switching between the transparent GP and opaque DS states at $T = 30$°C as the voltage $V = 30V_{\mathrm{rms}}$ is higher than $V_{\mathrm{DS}} = 24V_{\mathrm{rms}}$ at 100 Hz but lower than $V_{\mathrm{th}} = 54V_{\mathrm{rms}}$ at 300 Hz, as illustrated in Fig. 5.

The ambient temperature explicitly affects the EHD effect. Figure 6 shows the dependence of V_{DS} on f at $T = 20$°C, 30°C, and 40°C. Apparently, elevated temperature forced the transition voltage V_{DS} from the transparent to translucent state to shift to a higher f value. However, the virtually identical V_{DS} values ($\sim 20V_{\mathrm{rms}}$) at $f \leq 50$ Hz for the three curves imply that the required lowest excitation voltage to prompt EHD flow in the conduction regime at $f \ll f_c$ was practically independent of T. This phenomenon can be explained by Eq. (2), which unambiguously discloses negligible T dependence for V_{DS} as $f/f_c \ll 1$ although f_c actually decreases with decreasing T. One can also see from Fig. 6 that, at a fixed f value for operation, higher climate temperature entailed a lower V_{DS}.

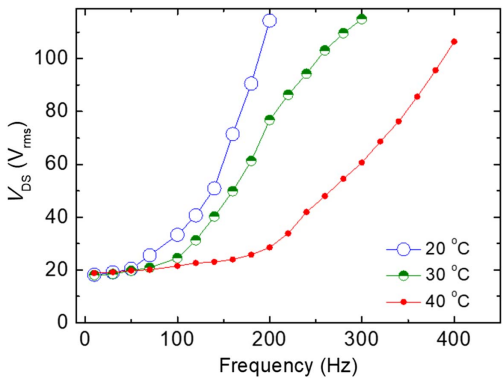

Fig. 6. Frequency-dependent voltage V_{DS} for the onset of the saturated opaque DS state of the CLC device measured at temperatures of 20°C, 30°C, and 40°C. V_{DS} grows monotonically as the applied frequency rises.

This finding can be easily understood because the higher thermal energy facilitates the ion movement as well as LC molecular motion.

Figure 7 unfolds the CLC device's alluring performance, showing T-dependent transmission at various operating voltages. It clarifies that the smart glass can preserve the transparent state at increased climate temperature, if one wishes, by operation with a higher f. For example, at voltage $30V_{rms}$ and frequency 100 Hz (blue solid line), the incident light will pass through the window (in the GP state) without scattering at temperatures below 20°C. When the temperature gets higher, light scattering takes place (in the DS state), and the scattering strength increases with increasing T until a saturated opacity is reached at around 30°C. The above-mentioned results corresponding to the blue T – T% curve in Fig. 7 undoubtedly confirm the proposed passive control scheme for thermo-responsive switching between the transparent GP at $T = 20$°C and opaque DS state at $T = 30$°C in Fig. 1(b). Obviously, the temperature to trigger switching from the tunable translucent to opaque state can be controlled electrically, providing a tunable or on-demand T_{DS}, at which T% decreases from ~80% to less than 1% (see, for example, the green curve in Fig. 7). It is worth mentioning that each T-dependent T% curve for an arbitrary voltage setting is completely reversible. Further, in comparison with the thermally passive and yet adaptive operation, driving voltage for amplitude-and-frequency, dual-active control assures the proactive manipulation of absolute authority as shown in Fig. 7 (as manifested by the exemplary black curve at $V = 100V_{rms}$ and $f = 100$ Hz). The transparent state can be recovered for sure upon removal of the voltage. Unlike previously reported smart windows possessing no capability of tunable temperature for the opaque state [18,19], the useful feature of adjustable T_{DS} demonstrated in this work offers the user full priority for active control and, as a consequence, is suitable for human inhabitants at all latitudes. This result greatly improves the practicality and convenience, where T_{DS} can be altered by a set of V and f values.

Figure 8 shows the T-varying appearance of a CLC test cell as our proposed smart glass situated in front of a flower by a distance of 70 cm. An IR camera was employed to monitor the real-time temperature variation in an outdoor environment. Uniformity of the haze was ascribed to the oblique heat flow from a hair dryer deflected from the line of sight to accommodate the IR camera. From 0 s to 20 s, the duration of thermal heating by the hair dryer is denoted by t in Fig. 8. Giving an electric voltage of $V = 50V_{rms}$ and $f = 300$ Hz (i.e., $T_{DS} = 50$°C to be in line with the condition for the red dashed-dotted curve in Fig. 7), one can clearly see the reduction in transmission of the cell over the temperature range of 29.8°C (at $t = 0$ s with uniform transparency in GP state) increasing to 52.6°C (at $t = 20$ s with uniform haze in DS state). Note that haze non-uniformity observed from the image at $T = 35.6$°C ($< T_{DS} = 50$°C) and $t = 10$ s or at $T = 42.8$°C ($< T_{DS} = 50$°C) and $t = 15$ s was temporary, which turned uniform as the temperature increased to 52°C ($> T_{DS} = 50$°C) at $t = 20$ s. This is due to the non-uniform temperature distribution in the cell produced by the oblique setting of the hair dryer that led to gradual expansion of DS domains from the bottom-right corner to the top-right corner with increasing t from 10 s to 20 s. Such temperature/time dependence of haze uniformity under a spatially non-uniform heating environment in Fig. 8 can be explained by the T – T% curve in Fig. 7 showing the thermally sensitive translucent DS state ($T_{th} < T < T_{DS}$) and temperature independence in the opaque DS state ($T > T_{DS}$). As a result, by taking advantage evidently shown in Fig. 7, one can still get uniform haze at $T = 35.6$°C or $T = 42.8$°C by varying either the voltage strength or frequency to adjust T_{DS}. From the point of view of large-scale application, the operation of the CLC device in the passive control mode would be unquestionably promising, but it would require a longer time to get full scattering for uniform haze in a larger screen when the heat flux on the cell plane is non-uniform.

Consequently, our efforts in confirming thermo-responsive transmission modulation by CLC state transitions of a voltage-

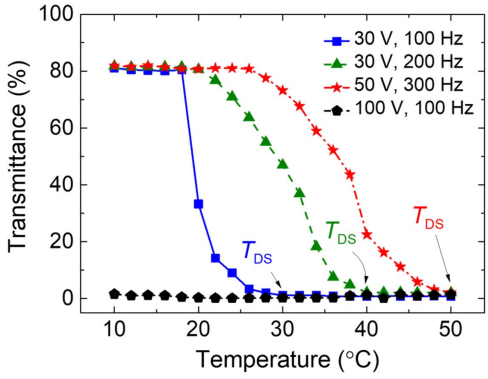

Fig. 7. Operating method of switching transmission from the GP state to highly DS state by raising temperature at fixed applied AC voltage and frequency values, $30V_{rms}$ at 100 Hz, $30V_{rms}$ at 200 Hz, $50V_{rms}$ at 300 Hz, and $100V_{rms}$ at 100 Hz. The switching temperature T_{DS} is determined as temperature-dependent transmittance falls to <1%.

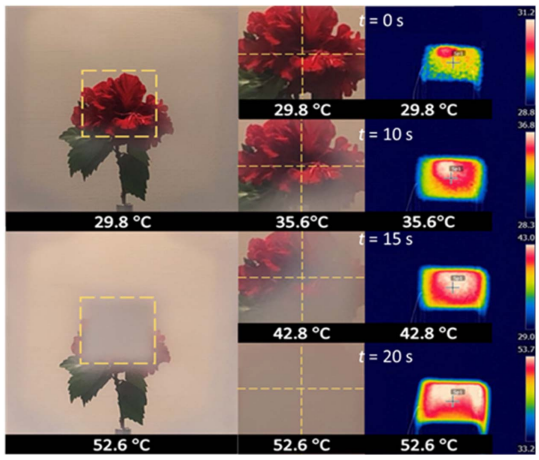

Fig. 8. Demonstration of the thermally adaptive smart control of the transmission of the CLC window at varying temperatures monitored by an IR camera. The China rose (*Hibiscus rosa-sinensis*) is 70 cm in distance behind the CLC cell, and the driving voltage condition corresponds to the red curve in Fig. 7 for which $V = 50V_{rms}$ and $f = 300$ Hz. t is the duration of thermal heating from the hair dryer.

sustained CLC cell in Fig. 7 and demonstrating self-shading of a real image from the transparent GP to opaque DS of the CLC cell in response to thermal variation in Fig. 8 serve well to support the mechanism of adaptive smart switching illustrated in Fig. 2(b). To further characterize the optical performance of the proposed dual-mode CLC smart glass in the visible light regime, haze values in different states (i.e., transparent GP state and voltage-sustained translucent and opaque DS states) were quantified by using a haze meter (Nippon Denshoku COH5500) to measure total (T_t%), specular (T_s%), and diffuse (T_d%) transmittance in the wavelength range of 400–700 nm. As defined by the instrument, T_s% (T_d%) is the relative transmission of light scattered at angles of less (greater) than 2.5° from the optical path, whereas T_t% is the sum of T_s% and T_d%. The value of T_t% through an empty cell in the GP state is set to 100%. The haze value can thus be calculated as the percentage ratio between T_d% and T_t% [i.e., $(T_d\%/T_t\%) \times 100\%$]. For operation of the cell in the active control mode, Fig. 9 reveals changes of T_t%, T_s%, and haze as functions of the 100-Hz voltage at $T = 30$°C. Analogous to the arbitrary V–T% curve in Fig. 4, the voltage-dependent T_t% properties in the entire visible range can be divided by two characteristic voltages of $V_{th} \sim 15V_{rms}$ and $V_{DS} \sim 25V_{rms}$ at 100 Hz (nearly the same as those indicated in Fig. 5) into three regions—the transparent GP state at $V < V_{th}$ with high transmittance of ~95%, grayscale translucent DS state at $V_{th} < V < V_{DS}$ with monotonous decrease in transmittance with increasing voltage, and opaque DS state at $V > V_{DS}$. The value of T_t% ~ 50% in the voltage-sustained opaque DS state obtained in Fig. 9 also connotes that nearly 50% of unpolarized light was backscattered at arbitrary angles from the CLC cell. As a result, referring to the schemes for operation of the CLC smart glass in the dual-active control mode in Fig. 1(a), the haze value is ~90% at $V = 30V_{rms}$ at 100 Hz in the DS state and ~0.1% at $V = 0V_{rms}$ or ~0.26% at $V = 30V_{rms}$ at 300 Hz in the GP state. Switching the CLC smart glass to the passive control mode, we measured the values of T_t%, T_s%, T_d%, and haze based on three dissimilar voltage-and-temperature conditions as given in Fig. 7. Table 1 shows that the optical properties (e.g., haze around 90%–91% as the representative) in the DS state are nearly of target-temperature (i.e., T_{DS}) invariance for the voltage-induced GP-to-DS transition. This assurance corroborates the superior electrical-active and self-adaptive features of the proposed device in both active and passive modes with reliable optical performances in the visible wavelength range and a wide working temperature range.

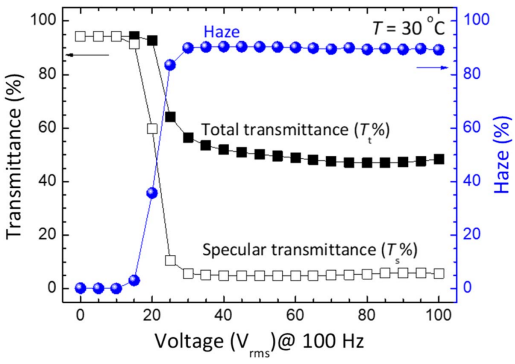

Fig. 9. Voltage dependence of the total transmittance (T_t%), specular transmittance (T_s%), and haze as measured by a haze meter in the visible range (400–700 nm) at $f = 100$ Hz and $T = 30$°C of the CLC smart glass in the active control mode.

Table 1. Optical Characteristics of Total Transmittance (T_t%), Specular Transmittance (T_s%), Diffuse Transmittance (T_d%), and Haze at Given Voltage and Temperature Conditions in Fig. 7 of the CLC Smart Glass in Passive Control Mode

Voltage Conditions	T (°C)/State	T_t%	T_s%	T_d%	Haze (%)
30 V at 100 Hz	20/GP	95.13	94.87	0.27	0.28
	30/DS	57.62	5.62	52.00	90.25
30 V at 200 Hz	20/GP	94.86	94.65	0.21	0.22
	40/DS	57.52	5.73	51.79	90.04
50 V at 300 Hz	20/GP	94.25	94.07	0.18	0.19
	50/DS	47.26	4.15	43.10	91.21

4. CONCLUSION

In summary, a smart window has been illustrated on the basis of the EHD effect in a negative CLC due to the contribution of ion motion and, in turn, flow of the anisotropic material in response to an excitation electric field oscillating at a low frequency. The transmission of the CLC sandwiched in a glass cell is thermo-responsive, automatically reducing its transparency by increased light scattering with increasing temperature to make the smart glass temperature adaptive. This device features a dual (i.e., voltage and frequency)-active control as well, enabling the smart glass to be electrically tunable and switchable among the transparent (GP), graded translucent (mild to moderate DS), and opaque (severe DS) states. The most intriguing characteristic of the CLC device reported in this study is that the temperature for a spontaneous state transition from one to another is fully adjustable or can be reset if is of default, prioritizing the electrically active or on-demand control over thermally passive control. The active and passive control of the CLC transmission is bidirectional, having no need of any further treatment or detour to regress to a previous gray level. As a proof of concept, Bragg reflection can be devised to sit in the NIR region so as to reject partial thermal radiation while keeping the CLC window optically transparent in the visible spectrum in the normal field-off state. The trade-off compared with an achiral LC system or a CLC with a longer pitch length is the relatively higher operating voltage. So far, while various LC-based technologies have been extensively demonstrated for active control of light transmission [9–13], options for passive-control purposes have still been limited and, in most cases, require the addition of certain thermo- or photo-responsive agents in designated LC systems [16,17]. Our present work achieves a substantial breakthrough of bridging this technical gap by exploiting the electrical and thermal tunability of EHD strength, embracing both active and passive operating modes for light intensity modulation in a simple architecture without the need of any stimuli-responsive substances for the device.

Funding. Ministry of Science and Technology, Taiwan (107-2112-M-009-012-MY3, 110-2112-M-A49-023).

Disclosures. The authors declare no conflicts of interest.

Data Availability. Data underlying the results presented in this paper are not publicly available at this time but may be obtained from the authors upon reasonable request.

REFERENCES

1. W. Helfrich, "Electrohydrodynamic and dielectric instabilities of cholesteric liquid crystals," J. Chem. Phys. **55**, 839–842 (1971).
2. Y. Sasaki, H. Hoshikawa, T. Seto, F. Kobayashi, V. S. Jampani, S. Herminghaus, C. Bahr, and H. Orihara, "Direct visualization of spatiotemporal structure of self-assembled colloidal particles in electrohydrodynamic flow of a nematic liquid crystal," Langmuir **31**, 3815–3819 (2015).
3. T. Kawakubo, A. Yanagita, and S. Kabashima, "External noise effect on the onset of Williams domain in nematic liquid crystals," J. Phys. Soc. Jpn. **50**, 1451–1456 (1981).
4. S. Hirata and T. Tako, "Optical properties of Williams domain," J. Appl. Phys. **21**, 675–679 (1982).
5. Z.-Y. Liang, C.-Y. Tu, T.-H. Yang, C.-K. Liu, and K.-T. Cheng, "Low-threshold-voltage and electrically switchable polarization-selective scattering mode liquid crystal light shutters," Polymers **10**, 1354 (2018).
6. Y. C. Hsiao and W. Lee, "Polymer stabilization of electrohydrodynamic instability in non-iridescent cholesteric thin films," Opt. Express **23**, 22636–22642 (2015).
7. Y.-L. Nian, P.-C. Wu, and W. Lee, "Optimized frequency regime for the electrohydrodynamic induction of a uniformly lying helix structure," Photon. Res. **4**, 227–232 (2016).
8. S. V. Serak, U. Hrozhyk, J. Hwang, N. V. Tabiryan, D. Steeves, and B. R. Kimball, "High contrast switching of transmission due to electrohydrodynamic effect in stacked thin systems of liquid crystals," Appl. Opt. **55**, 8506–8512 (2016).
9. Y. Zhan, H. Lu, M. Jin, and G. Zhou, "Electrohydrodynamic instabilities for smart window applications," Liq. Cryst. **47**, 977–983 (2019).
10. Z. Lan, Y. Li, H. Dai, and D. Luo, "Bistable smart window based on ionic liquid doped cholesteric liquid crystal," IEEE Photon. J. **9**, 2200307 (2017).
11. C.-W. Chen, A. N. Brigeman, T.-J. Ho, and I. C. Khoo, "Normally transparent smart window based on electrically induced instability in dielectrically negative cholesteric liquid crystal," Opt. Mater. Express **8**, 691–697 (2018).
12. X. Xie, P. Huang, M. Xu, Y. Ding, L. Qiu, and H. Lu, "Tri-state switching of a high-order parameter, double-layered guest-host liquid-crystal shutter, doped with the mesogenic molecule 4HPB," Liq. Cryst., 1–6 (2021).
13. K. Goda and R. Yanagi, "Active anti-glare device for smart windows based on electrohydrodynamic instability in liquid crystals," Mol. Cryst. Liq. Cryst. **711**, 1–7 (2021).
14. Y. Zhang, X. Yang, Y. Zhan, Y. Zhang, J. He, P. Lv, D. Yuan, X. Hu, D. Liu, D. J. Broer, G. Zhou, and W. Zhao, "Electroconvection in Zwitterion-doped nematic liquid crystals and application as smart windows," Adv. Opt. Mater. **9**, 2001465 (2020).
15. J.-W. Huh, J.-H. Kim, S.-W. Oh, S.-M. Ji, and T.-H. Yoon, "Ion-doped liquid-crystal cell with low opaque-state specular transmittance based on electro-hydrodynamic effect," Dyes Pigment **150**, 16–20 (2018).
16. S.-W. Oh, S.-H. Kim, J.-M. Baek, and T.-H. Yoon, "Optical and thermal switching of liquid crystals for self-shading windows," Adv. Sustain. Syst. **2**, 1700164 (2018).
17. Y. Zhan, A. P. H. J. Schenning, D. J. Broer, G. Zhou, and D. Liu, "Light-driven electrohydrodynamic instabilities in liquid crystals," Adv. Funct. Mater. **28**, 1707436 (2018).
18. D. Cupelli, F. Pasquale Nicoletta, S. Manfredi, M. Vivacqua, P. Formoso, G. De Filpo, and G. Chidichimo, "Self-adjusting smart windows based on polymer-dispersed liquid crystals," Sol. Energy Mater. Sol. Cells **93**, 2008–2012 (2009).
19. R. Bao, C.-M. Liu, and D.-K. Yang, "Smart bistable polymer stabilized cholesteric texture light shutter," Appl. Phys. Express **2**, 112401 (2009).
20. H. Khandelwal, R. C. Loonen, J. L. Hensen, M. G. Debije, and A. P. Schenning, "Electrically switchable polymer stabilised broadband infrared reflectors and their potential as smart windows for energy saving in buildings," Sci. Rep. **5**, 11773 (2015).
21. H. Khandelwal, M. G. Debije, T. J. White, and A. P. Schenning, "Electrically tunable infrared reflector with adjustable bandwidth broadening up to 1100 nm," J. Mater. Chem. A **4**, 6064–6069 (2016).
22. H. Khandelwal, R. C. Loonen, J. L. Hensen, A. P. Schenning, and M. G. Debije, "Application of broadband infrared reflector based on cholesteric liquid crystal polymer bilayer film to windows and its impact on reducing the energy consumption in buildings," J. Mater. Chem. A **2**, 14622–14627 (2014).
23. G. H. Heilmeier, L. A. Zanoni, and L. A. Barton, "Dynamic scattering: a new electrooptic effect in certain classes of nematic liquid crystals," *Proc. IEEE Inst. Electr. Electron. Eng.* **56**, 1162–1171 (1968).
24. Orsay Liquid Crystal, "AC and DC regimes of the electrohydrodynamic instabilities in nematic liquid crystals," Mol. Cryst. Liq. Cryst. **12**, 251–266 (2007).
25. J. P. Hurault, "Static distortions of a cholesteric planar structure induced by magnetic or ac electric fields," J. Chem. Phys. **59**, 2068–2075 (1973).
26. F. Rondelez, H. Arnould, and C. J. Gerritsma, "Electrohydrodynamic effects in cholesteric liquid crystals under ac electric fields," Phys. Rev. Lett. **28**, 735–737 (1972).